Monitoring of Beams in an RC Building during a Load Test Using Distributed Sensors

Andre Brault[1]; Neil A. Hoult, M.ASCE[2]; Tom Greenough[3]; and Ian Trudeau[4]

Abstract: The understanding of the complex behavior of reinforced concrete elements in situ would be aided if distributed strain measurements were captured during load tests, potentially leading to more accurate assessments and load ratings, and optimized future designs. This research investigates the use of distributed fiber optic sensors (FOS) to monitor three beams in a newly constructed RC building during a load test. It is the first case where an FOS technique capable of monitoring distributed strains, distributed deflections, and crack widths simultaneously is implemented in the field. The FOS data captured inflection points, moment transfer at the supports, crack locations, and crack openings. The FOS also captured deflected shapes, enabling maximum deflections to be determined without prior knowledge of where they would occur. Lastly, the measured results from the load test were compared to design model predictions for each element.
DOI: 10.1061/(ASCE)CF.1943-5509.0001250.

Author keywords: Distributed fiber optic sensors; Load tests; Reinforced concrete; Concrete cracks; Strain; Deflections; Monitoring; Serviceability; Buildings.

Introduction

In recent years, the quantity of greenhouse gas emissions caused by building operation has been reduced substantially; however, the quantity of emissions caused by construction itself is still increasing (Allwood and Cullen 2012). This suggests that there is an opportunity for structural engineers to help the environment through the optimization of material use in building construction and design. In many structures there is also beneficial structural behavior not initially assumed to be present using computational models (Tumialan et al. 2014). If this beneficial behavior in existing reinforced concrete structures could be understood in detail, this knowledge could be used to optimize their design in the future. Additionally, it may enable the load rating of existing structures to be increased allowing them to be kept in service or even repurposed rather than demolished, further reducing the impact on the environment.

Protocols for load testing existing RC buildings are described in Chapter 20 of ACI 318 (ACI 2014a) and ACI 437.2 (ACI 2014b), and these protocols have been followed in various research studies (Casadei et al. 2005; Galati et al. 2008; De Luca et al. 2013). Casadei et al. (2005) performed a load test on RC elements in situ and found that the factored design loading amounted to typically only 80% of the true ultimate capacity. Furthermore, a study performed by De Luca et al. (2013) found that the ultimate capacities of RC slabs tested to failure in situ were up to four times larger than the factored design loads in accordance with ACI load testing protocols. Currently, it is not uncommon for RC buildings to be stronger than required (Tumialan et al. 2014), which in turn indicates that these structures could have served their function using less material.

However, the reasons for the reserve strength are not always clear as the instrumentation used to monitor these RC structures was comprised solely of discrete sensors, which can miss important localized behavior. For example, a measurement of the midspan displacement of a beam might indicate that the beam is stiffer than expected but does not provide any information as to why. Or a strain gauge placed on the surface of a beam at midspan could measure very low strains if placed near a crack when in fact the strains elsewhere in that region could be critical. In fact, all of the instrumentation devices that ACI Committee 437 suggests be used during a load test are discrete technologies, such as strain gauges, extensometers, and linear variable differential transformers (LVDTs) (ACI 2003). Without capturing a detailed distributed set of measurements during a load test it is difficult to diagnose the causes of an RC element's overdesign as cracking characteristics, shrinkage, creep, loading history, and support conditions all play an important role when considering in situ RC behavior (Bischoff 2005). Furthermore, the process of performing a load test is expensive and requires significant planning to be successful, thus it is important to capture as much data as is feasibly possible. Scott et al. (2002) installed 163 strain gauges to capture distributed strains along the internal reinforcement within a flat slab in a full-scale RC building in the Large Building Test Facility of the Building Research Establishment (Cardington, UK). However, intensive instrumentation programs of this nature are often impractical to implement in the field.

Regier and Hoult (2014) found that distributed fiber optic sensors (FOS) are a feasible technology to implement in the field, as they successfully used FOS to monitor distributed strains on an RC bridge in Ontario, Canada, during a load test. Bentz and Hoult (2016) later used this FOS data to perform a model updating exercise. The initial model predicted displacements that were an order of magnitude conservative compared to the deflections measured

[1]Researcher, Dept. of Civil Engineering, Queen's Univ., 58 University Ave. Kingston, ON, Canada K7L 3N6. Email: andre.brault@queensu.ca

[2]Associate Professor, Dept. of Civil Engineering, Queen's Univ., 58 University Ave. Kingston, ON, Canada K7L 3N6 (corresponding author). Email: neil.hoult@queensu.ca

[3]Associate, Entuitive Corp., 200 University Ave., 7th Floor, Toronto, ON, Canada M5H 3C6. Email: tom.greenough@entuitive.com

[4]Associate, Entuitive Corp., 200 University Ave., 7th Floor, Toronto, ON, Canada M5H 3C6. Email: ian.trudeau@entuitive.com

Note. This manuscript was submitted on February 28, 2018; approved on July 30, 2018; published online on November 22, 2018. Discussion period open until April 22, 2019; separate discussions must be submitted for individual papers. This paper is part of the ***Journal of Performance of Constructed Facilities***, © ASCE, ISSN 0887-3828.

by a displacement transducer during the load test. In this case, Bentz and Hoult (2016) found that the detailed measurements captured by the FOS allowed them to determine that the support conditions and surrounding soil pressures were what led to the bridge's unexpected increased structural response. This is a promising example, as the FOS provided information regarding the bridge's behavior that a typical instrumentation configuration could not. In addition to the distributed strains captured in this instance, the FOS data was also used to estimate full deflected shapes (Regier and Hoult 2014) and concrete crack widths (Bentz and Hoult 2016). However, the methods used to determine both had not yet been validated, which is important to note as both crack widths and flexural deflections are crucial serviceability criteria.

The serviceability performance of RC structures is particularly difficult to predict in design and analysis, as cracking behavior, shrinkage, creep, and tension stiffening are all complex phenomenon that can affect the prediction [ACI 209.2R (ACI 2008)]. Because of this, ACI Committee 437 recommends that deflections, crack widths, and crack spacings be measured during a load test when assessing serviceability of flexural RC elements [ACI 437R (ACI 2003)]. A technique of using distributed FOS to measure RC beam deflections, crack widths, crack spacing, and external concrete surface strains simultaneously was developed by Brault and Hoult (2018), though this technique has not yet been implemented in the field. If this technique were used to monitor RC buildings in the field, it could capture in situ behavior at a level of detail that has not been previously achievable, providing invaluable data for serviceability assessment, model calibration, and determining the causes of overdesign such as conservative assumptions about support conditions and load distribution.

In light of this introduction, the objectives of this research are as follows: (1) monitor RC beams in a building during a load test using distributed FOS; (2) analyze the distributed FOS strain data to determine distributed deflections, crack widths, crack spacing, and support conditions; and (3) compare the measured field data to design model predictions.

Field Monitoring of RC Structures with Fiber Optic Sensors

FOS have the advantages of being low cost, small, embeddable within concrete, and immune to electrical magnetic interference (Li et al. 2004). The monitoring of structures with FOS layouts provides an opportunity to not only detect deterioration but also optimize existing service lives and new designs (Merzbacher et al. 1996). The following section will discuss previous field monitoring research that has been conducted on concrete structures (specifically bridges and buildings) using three types of FOS technologies: (1) fiber Bragg gratings, (2) Brillouin backscattering, and (3) Rayleigh backscattering.

Fiber Bragg gratings (FBG) are a type of discrete fiber optic sensor that provide advantages over conventional electrical resistance strain gauges as they are intrinsically stable. Thus they have the capability to provide long-term measurements without experiencing drift and can be used in harsh environments (Gebremichael et al. 2005). The Taylor Bridge (Manitoba) was instrumented with 63 FBG sensors to measure maximum strains within the girders. In this case, 60% of the conventional strain gauges installed were damaged during the concrete curing process yet all fiber optic sensors installed survived (Maaskant et al. 1997). Research performed by Gebremichael et al. (2005) investigated the performance of Europe's first concrete bridge entirely reinforced with fiber-reinforced polymers (FRP) through the installation of 40 FBG sensors. The sensors monitored the structural integrity of the bridge, and the strain results were validated against the results of conventional gauges. Though research investigating the monitoring of RC bridges with FBGs is extensive, there is limited literature reporting any monitoring campaigns using FBG sensors in RC buildings other than cases where only foundation piles are instrumented (Majumder et al. 2008). However, there has been research on FBGs applied to RC elements in the laboratory (Majumder et al. 2008), as well as steel buildings (Li et al. 2004).

Brillouin optical time domain reflectometry (BOTDR) systems provide distributed measurements over long sensing lengths (several kilometers) with a minimum spatial resolution and accuracy of approximately 0.5 m and 35 $\mu\varepsilon$, respectively (Mohamad et al. 2011). Brillouin-based FOS, like FBG sensors, have been installed in several RC bridge projects. For example, fiber optic readings recorded at the Musmeci Bridge (Italy), an RC bridge, found that cracks caused by thermal loading of the bridge could be detected over a 1 year monitoring period (Minardo et al. 2012). Bastianini et al. (2007) monitored two RC bridges in Missouri and found that although the results correlated well with theoretical predictions, the presence of concrete cracks led to discrepancies between the FOS and conventional strain gauges. Brillouin systems have been installed on the internal reinforcement of beams in a large RC building as well (Ohno et al. 2001). It was found that internal reinforcement strains could be measured without water proofing and surface preparation, which is typically required with conventional strain gauges.

Rayleigh backscatter measurement systems provide distributed measurements with spatial resolutions as low as 5 mm and accuracies as high as 1 $\mu\varepsilon$ (Gifford et al. 2007). However, with this technology the maximum sensing length is usually less than 100 m (Gifford et al. 2007). Rayleigh systems have been used to monitor several RC elements in the laboratory (Regier and Hoult 2015; Villalba and Casas 2013; Billon et al. 2015), though to the author's knowledge there is only one example of Rayleigh backscattering being used to monitor an RC bridge or building in the field. Regier and Hoult (2014) installed external FOS on the surface of four girders at the Black River Bridge (Ontario, Canada), where they gained critical insights into the bridge's support conditions, stiffness, cracking behavior, and load sharing during the performance of a live load test. There is still a need to monitor an RC building with a Rayleigh backscattering FOS system as this can provide detailed measurements allowing for better understanding of structural behavior and building interaction that is not currently achievable.

The specific distributed FOS analyzing unit that is used in the following study is the OBR4600 from Luna Technologies [also used by Regier and Hoult (2014) when monitoring the Black River Bridge], which uses Rayleigh backscatter measurements to acquire strain readings with an accuracy of 1 $\mu\varepsilon$ and a maximum total fiber length of 70 m (Luna Technologies 2011). Note that the OBR4600 cannot measure strain and temperature independently. The effects of temperature changes on the FOS strain readings can be mitigated if the testing environment has a constant temperature during the test (Regier and Hoult 2014). If long-term monitoring is desired (not performed in this study), strategies employed by previous researchers (e.g., Mohamad et al. 2011) to compensate for temperature effects on FOS strain readings should be used. The type of fiber optic cable used is a single-mode fiber (core diameter of 8 μm) wrapped in a nylon coating, which is commercially available for ~\$0.15/m. Regier (2013) determined that this fiber optic cable, when bonded to the concrete surface with the two-part Loctite E 20-HP adhesive, provides the most accurate results when measuring concrete strains, and further has the ability to bridge cracks on the concrete surface. However, the bridging of concrete cracks is

only possible due to slip between the nylon coating and the inner sensor core, as the nylon coating is only bonded to the fiber core via friction (Hoult et al. 2014). This is important, as it results in an averaging of measured strains in the vicinity of a concrete crack (Regier and Hoult 2014).

Experimental Program

Field Monitoring Site

The load testing was performed during the construction of the Rideau Centre Expansion in Ottawa, Ontario, Canada. The Rideau Centre Expansion is a large RC building that was completed in 2016 and is comprised of seven floors of reinforced concrete slabs with dimensions of approximately 80×80 m, with a floor to floor height of 5 m. There are two slabs below ground (Levels P1 and P2), one at ground level (Level 1), and four slabs above ground (Levels 2, 3, 4, and the roof slab). The load testing performed took place on Level 4 of the building. A plan-view schematic of Level 4 is shown in Fig. 1(a), which indicates the two zones on Level 4 where load testing was performed: Zone A and Zone B. The building has a typical column spacing of 9×9 m, has several shear walls, and has two large oval openings on Level 4 [Fig. 1(a)].

Three cast-in-place RC elements were instrumented and tested. In Zone A [Fig. 1(b)], a beam and a drop panel were instrumented, which are located on column bays next to each other (these elements will be referred to as the beam and the drop from here on). In Zone B [Fig. 1(c)] a larger beam was instrumented, which is oriented at an angle of 34° from the building's grid (and will be referred to as the large beam from here on). The beam, the drop, and the large beam were constructed with concrete designed to have a compressive strength of 30 MPa.

The beam and the drop [Fig. 1(b)] both have column-center to column-center spans of 13 m with a 4.5 m cantilever extending toward the southern edge of the building. The RC columns that support both the beam and drop have dimensions of 600×600 mm. The concrete slab on top of both the beam and the drop has a thickness of 300 mm, and the depth of the beam and the drop including the slab are 1,100 and 700 mm, respectively. The width of the beam and drop are 600 and 3,000 mm, respectively. The large beam [Fig. 1(c)] has a column-center to column-center span of 16.2 m, and the columns supporting the large beam are steel, with the north column being a $W360 \times 421$ section and the south column being a $W360 \times 634$ section. There is a beam that frames into the large beam 5.2 m south of the north column. The concrete slab has a thickness of 250 mm east of the large beam. West of the large beam, the concrete slab has a thickness of 300 mm north of the beam framing in and a thickness of 400 mm south of the beam framing in. The depth of the large beam (slab included) is 1,000 mm and the width is 2,000 mm.

Fiber Optic Instrumentation

Distributed fiber optic sensors were installed on the surface of the RC elements 3 months following concrete placement when all formwork, shores, and reshores had been removed. The FOS installation process included the following steps: (1) sanding of the fiber pathway with a 150 grit wheel, (2) cleaning the fiber pathway with water and 99% isopropyl alcohol, and (3) bonding the FOS to the concrete surface using the two-part adhesive Loctite E-20HP.

The FOS layout on the beam and the drop is shown in Figs. 2(a and b). The fibers were installed on the west side of each element in the longitudinal direction at two separate heights. The fibers were bonded to the concrete surface from the center of the north column to midspan (6.5 m from the center of the north column). At midspan, the FOS were looped such that a single fiber optic cable was used for the top and bottom instrumentation. The top fiber pass was installed 75 mm below the bottom of the concrete slab soffit, while the bottom fiber pass was installed 75 mm above the bottom edge of both the beam and the drop. The FOS instrumentation in both cases did not extend beyond midspan due to construction obstacles present at the field site.

The FOS layout installed on the large beam is shown in Fig. 2(c). The fibers were installed to the west side of the large beam at two separate heights. The fibers were bonded from the center of the north column to 0.34 m north of the south column's inner edge. When the instrumentation was being installed on the large beam, a pipe installed on the surface of the beam 11.9 m away from the north column provided an obstacle, which prohibited both the top and fiber passes from being installed between 11.7 and 12.1 m away from the north column. Furthermore, the beam framing into the large beam 5 m away from the north column provided another obstacle, and the top fiber pass could not be installed between 4.2 and 5.8 m away from the north column. The bottom fiber was installed 75 mm above the bottom edge of the large beam, while the top fiber was installed 75 mm below the soffit of the floor slab. The large beam's FOS instrumentation was not fully extended to the center of the south column once again due to a physical obstacle. Fig. 3 shows the large beam during the instrumentation process.

Load Test Setup and Procedure

The load tests performed on the beam, the drop, and the large beam were done 4 months following concrete placement. The test setup for each is shown in Fig. 4. The loading was performed using six scissor lifts: four weighing 11.5 kN (L1), one weighing 15.9 kN (L2), and one weighing 15.6 kN (L3). The scissor lifts were driven into place one at a time. A linear potentiometer (LP) was installed in each case to measure midspan deflections; however, in the case of the beam the LP was installed 300 mm north of midspan due to a physical obstacle. The LP used was a 24 mm subminiature gauging differential variable reluctance transducer (DVRT) from LORD Microstrain with a measurement accuracy of ± 0.024 mm and a stroke of 24 mm (Lord Microstrain 2015). The LP was set to continuously log displacement measurements throughout each load test at 1 Hz.

An OBR4600 was used to take FOS strain measurements, which is not capable of taking strain measurements dynamically. Thus, FOS readings were only taken at certain load stages during each test. For the beam and the drop, FOS readings were taken at the following load stages: (1) prior to loading, (2) when the middle two scissor lifts were in place, (3) when all six scissor lifts were in place, and (4) once all scissor lifts had been removed. FOS readings were taken for the large beam at the same load stages except for load Stage 2, which was not performed due to time constraints. The OBR4600 was set to take strain measurements with a gauge length and sensor spacing of 20 mm, as this was found by Brault and Hoult (2018) to provide the most accurate results when strains are expected to remain below 200 $\mu\varepsilon$ (which is the case in this study). Because the duration of each load test was under 1 h and the internal temperature of the construction site was controlled, temperature fluctuations were minimal and were thus assumed to have a negligible effect on the FOS strain readings (eliminating the need for temperature compensation of the FOS strain readings).

As shown in Figs. 4(a and b), the scissor lifts were oriented perpendicular to the longitudinal axis of both the beam and the

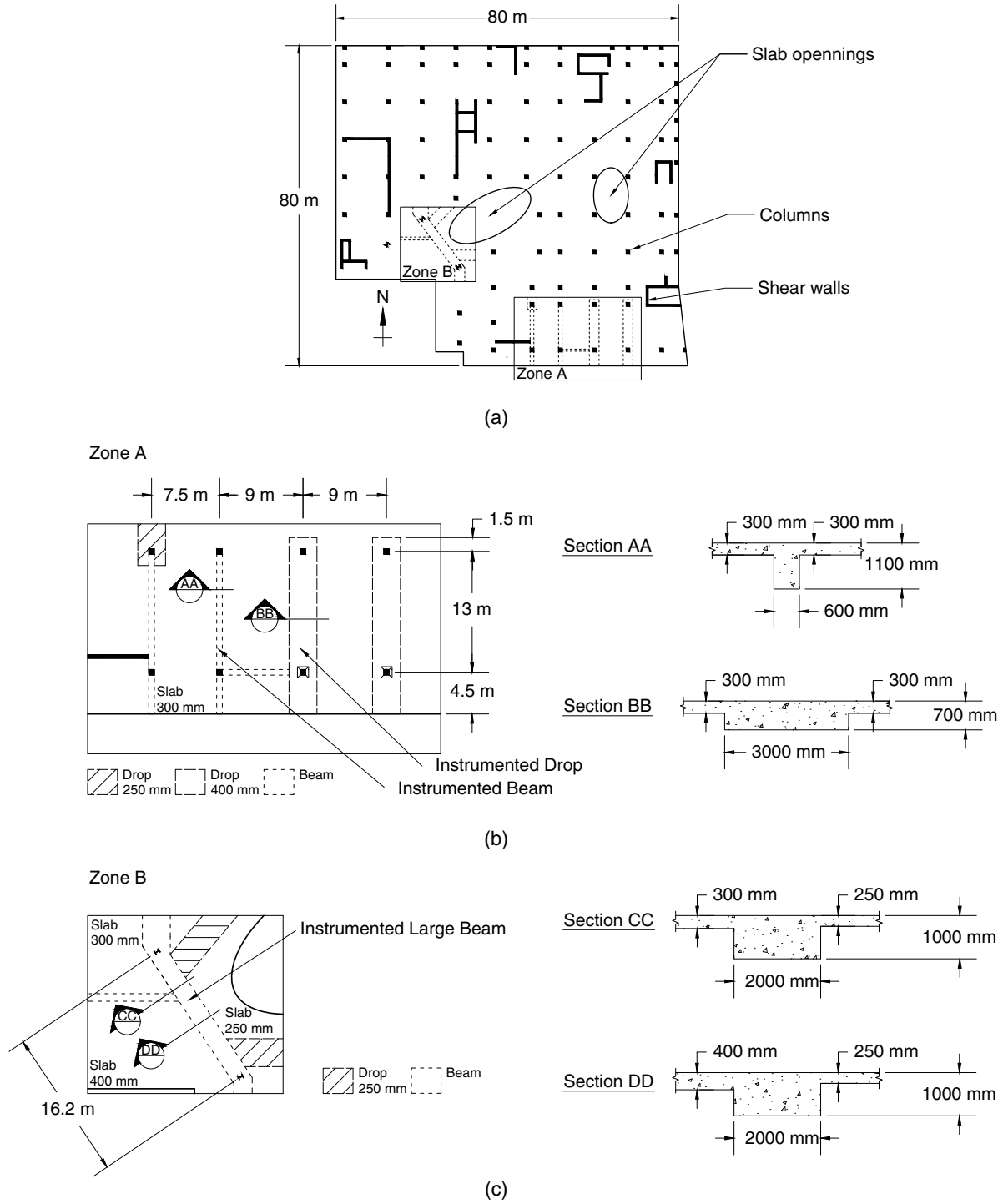

Fig. 1. Plan view of Level 4: (a) full level including Zone A and Zone B; (b) Zone A including the beam and drop; and (c) Zone B including the large beam.

drop. This was done in an effort to concentrate the loads at midspan to maximize the loading effects of the test. In Fig. 4(c), one can see that the scissor lifts were oriented in line with the large beam's longitudinal axis. This was due to shoring in the vicinity of the large oval slab opening (Fig. 1) not allowing the scissor lifts to be oriented perpendicular to the longitudinal axis while also being centered on top of the large beam. It is seen that the load magnitudes are not symmetrical about midspan in any test setup. This was not intentionally done, but was a result of the exact differences in weight between each scissor lift type (L1, L2, and L3) not being precisely known during testing.

Note that the loads applied in these tests were less than the unfactored design live load for each element. Line load approximations of the unfactored design live load (4.8 kPa) based on the tributary width for the beam, the drop, and the large beam are 40, 43, and 58 kN/m, respectively. If the scissor lift loads are approximated as line loads they are equivalent to 38% (15 kN/m), 35% (15 kN/m), and 12% (7 kN/m) of the unfactored design live loads

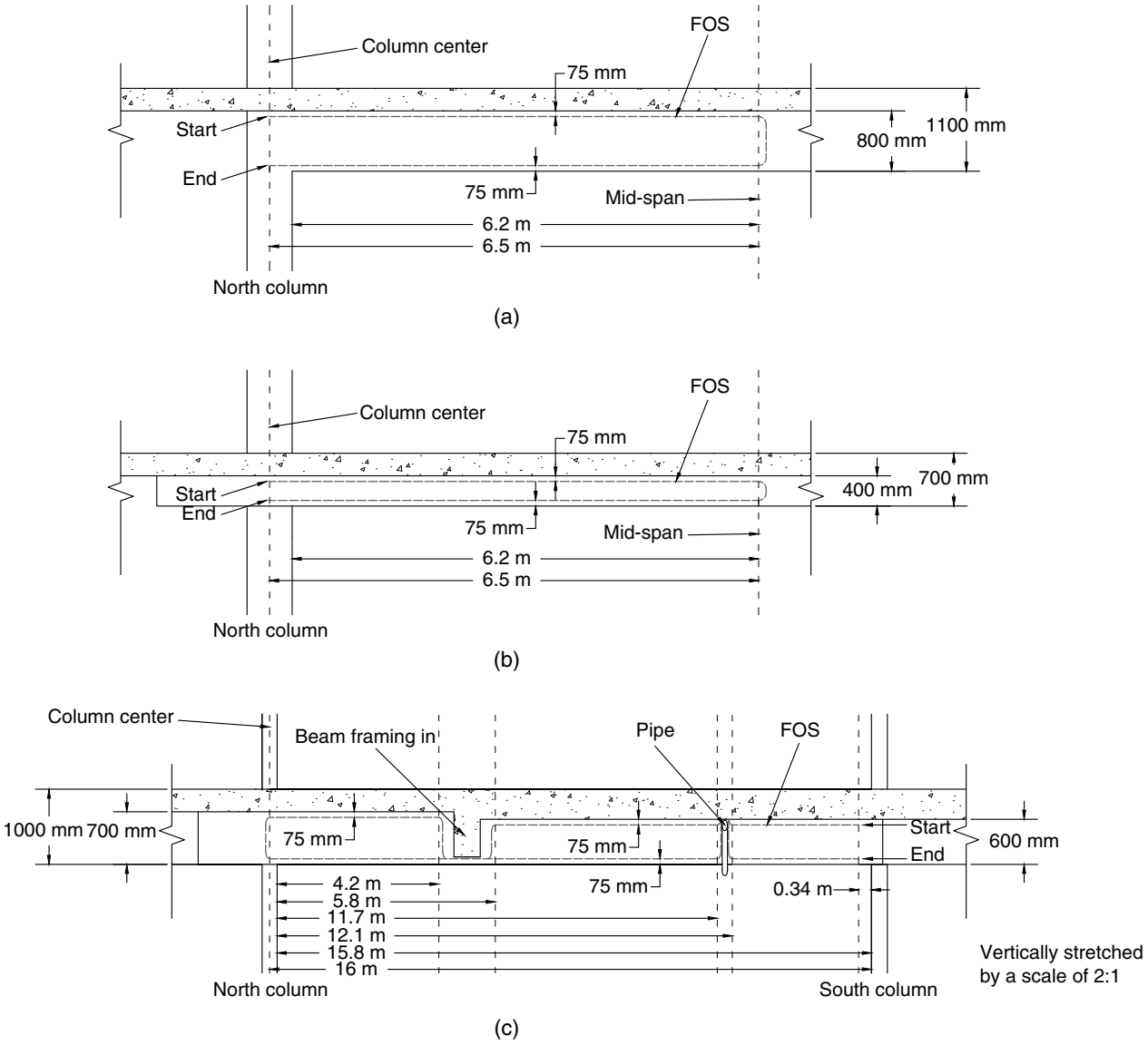

Fig. 2. Elevation view of the FOS instrumentation: (a) beam; (b) drop; and (c) large beam.

for the beam, the drop, and the large beam, respectively. Note that these scissor lift line loads do not act along the entire span of each element but solely on the middle of span where the scissor lifts are located, while the design line load is assumed to act on each element's entire span.

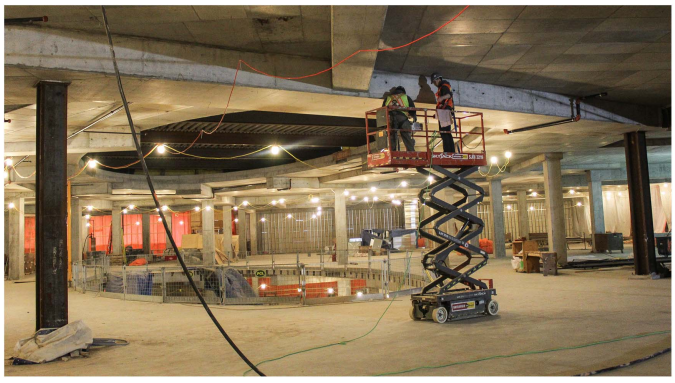

Fig. 3. Large beam during FOS installation.

Results and Discussion

Distributed Strains

FOS strain measurements are presented in Fig. 5 for all three elements loaded with six scissor lifts (loading configurations shown in Fig. 4). In both the beam [Fig. 5(a)] and the drop [Fig. 5(b)] the bottom fiber measures the largest tensile strain magnitudes and these occur near each element's midspan (6,500 mm), which is expected in positive bending as the bottom fibers are located near the element's extreme tensile fiber. In each part of Fig. 5, the large tensile strain peaks in the figure indicate the location of cracks opening on the concrete surface beneath the fiber (and are labeled as *Cracks in concrete surface*), which has been confirmed by other researchers using the OBR4600 (Regier and Hoult 2014; Villalba and Casas 2013). From this, the cracked regions, the crack spacing, and the magnitude of crack openings can be deduced (as is discussed in the next section). Compressive strains are measured in the bottom fibers near the support (north column), indicating the presence of negative bending at the north column and thus providing insight into the support conditions. The presence of negative bending at

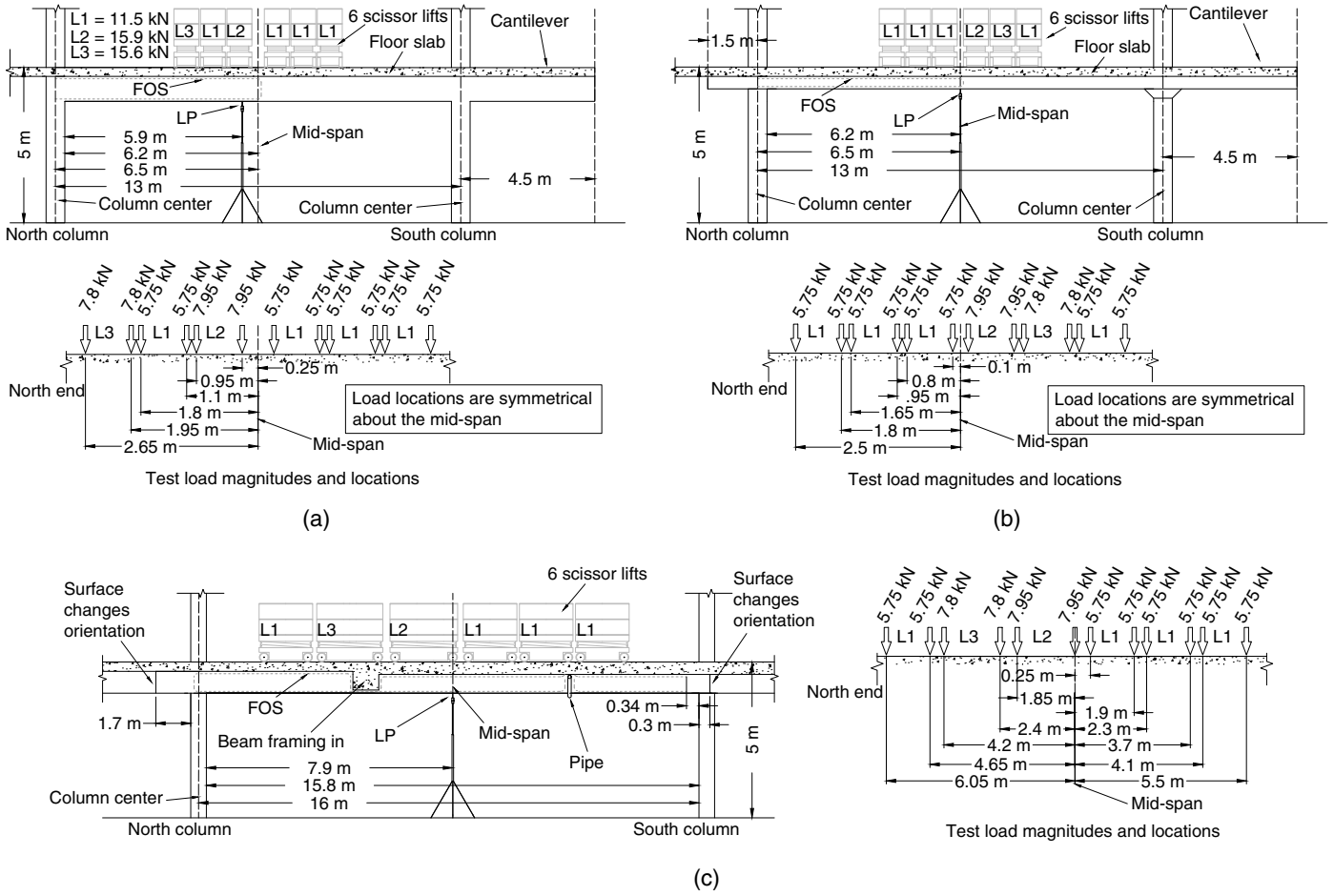

Fig. 4. Elevation view of the load test setups: (a) beam; (b) drop; and (c) large beam.

the north column suggests that moment is transferred into either the north column itself or the slab that continues north of the column. Because FOS were not installed on the columns or the slabs north of the columns, the exact moment distribution at the connection cannot be determined.

For the beam and the drop, the top fiber strain measurements appear to measure strains near a value of 0 $\mu\varepsilon$ for approximately the first 3,000 mm, suggesting that the top fiber is located very near to the cross section's neutral axis in this portion of both elements. However, beyond this point, cracks are seen in the bottom fiber measurements and the top fiber measurements begin to measure tensile strains as well, indicating that the top fiber is located below the neutral axis in the cracked portions of each element. Once again, this behavior makes sense as the neutral axis is expected to be higher in areas where the elements are cracked. A critical characteristic of each element's behavior that can also be determined is the location of the inflection point, which occurs where the top and bottom fiber strain measurements intersect. The inflection points (where the strain changes from compressive to tensile as indicated by the *Inflection point* labels in Fig. 5) were found to be located at 1,620 and 2,340 mm from the center of the north column for the beam and the drop, respectively. This provides insight into the support conditions once again, and suggests that the level of moment transfer present at the north column of the drop is slightly higher than seen for the beam. This is potentially explained by the fact that the drop itself extends 1.5 m north of the north column while the beam does not (Fig. 1).

In theory, the concrete surface strains at the edge of a crack are zero, while the strain across a crack is infinite. Though the FOS is able to bridge the concrete crack openings, the FOS does not measure the true concrete surface strains in the vicinity of a crack, but rather measures average strains due to slip between the fiber's nylon coating and the sensing core (Regier and Hoult 2014). However, the average strain measurements are important as they allow for crack widths/openings to be measured (discussed in the next section) and also provide critical data for concrete modeling theories that utilize average strains such as the modified compression field theory (MCFT) (Vecchio and Collins 1986). Previous laboratory work by Regier (2013) has shown that the FOS concrete surface strain measurements match conventional strain gauges when in an uncracked portion of concrete. Typically, FOS concrete surface strain measurements at least 100 mm away from a concrete crack are accurate (Regier and Hoult 2014). Thus, the measured strains for both the beam and the drop near their supports should be the true concrete surface strains. The maximum magnitudes of the measured concrete strains near the supports are -5 and -4 $\mu\varepsilon$ for the beam and drop, respectively. Because of the OBR4600's measurement accuracy (~1 $\mu\varepsilon$), these measurements still provided useful information despite the low strain magnitudes induced. It is also important to note that other distributed FOS systems, such as BOTDR, are reported to have accuracies of 30–38 $\mu\varepsilon$ (Ohno et al. 2001; Mohamad et al. 2011), and thus would not effectively measure the beam and drop behavior in this case.

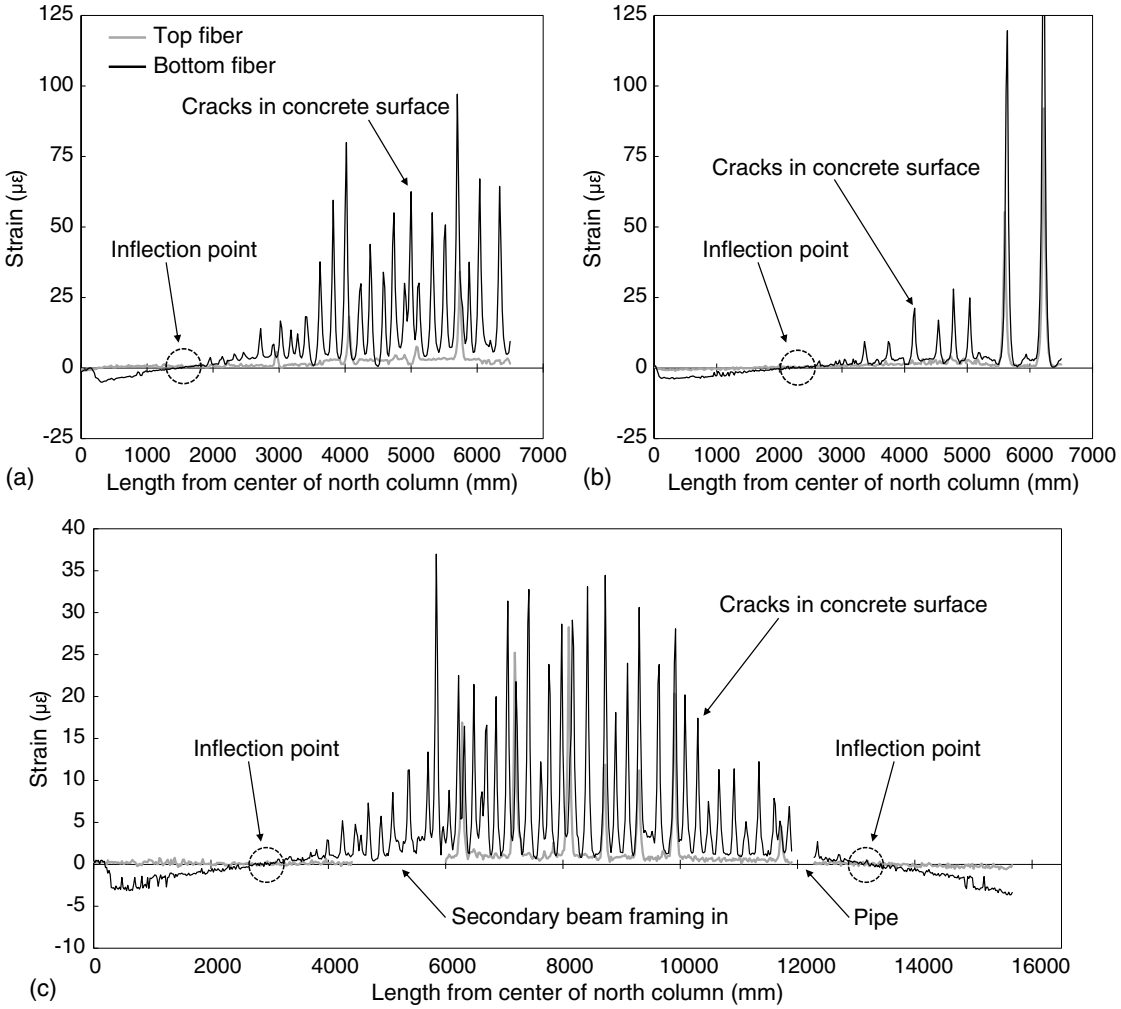

Fig. 5. FOS strains due to six scissor lifts: (a) beam; (b) drop; and (c) large beam.

FOS strain results from the large beam loaded with six scissor lifts are shown in Fig. 5(c). Portions of the large beam FOS strain results are missing (shown as gaps in the strain data and labeled as *Secondary beam framing* in and *Pipe*) due to the obstacles shown in Fig. 2(c). Furthermore, FOS measurements were only taken up until 15,660 mm, which is 340 mm away from the inner edge of the south column (16,000 mm), as FOS were only installed up until this point due to a physical obstacle on site. Once again as expected in positive bending, the largest tensile strains are measured near midspan (8,100 mm) in the bottom fiber with large strain peaks seen in this region as well due to concrete cracks. Near both supports, the bottom fiber measures compressive strains of -3 to -4 $\mu\varepsilon$, signifying that negative moments are present at the supports and that there is some moment transfer into either the columns or the surrounding slabs continuing beyond both columns. The top fiber measures essentially zero strain in the portions of the beam that are uncracked, while it measures slight tensile strains ($\sim$1 $\mu\varepsilon$) in the cracked region between cracks, again indicating that the top fiber is located at the beam's neutral axis near the supports and slightly below the neutral axis in the cracked portion of the beam. The inflection points are found to be at 3,000 and 13,240 mm (2,960 mm away from the center of the south column), indicating that comparable support conditions exist at both columns. Despite only applying a live load amounting to approximately 12% of the unfactored design live load, and measuring a maximum tensile strain of just 37 $\mu\varepsilon$ (at 5,840 mm), the FOS system used in this study was still able to provide detailed information regarding the large beam's behavior in terms of the induced strains, support conditions, and crack locations.

Cracking Behavior

The FOS measure large tensile strain peaks when bridging concrete cracks as previously discussed. Knowing this, the location of the cracks on each RC element can be determined, allowing for properties such as the average crack spacing and the length of the cracked region to be measured. Due to the sensor spacing of 20 mm, the location of each crack on the RC elements tested can be determined to be within 20 mm of its true location. Furthermore, Brault and Hoult (2018) have shown that the FOS strain measurements from RC elements using the OBR4600 and a nylon coated fiber optic cable can be used to measure crack widths. Using this technique to measure crack widths, the amount that each crack width has increased due to the load testing can be determined.

The location of each concrete crack at the height of the bottom fiber and the amount that each crack has opened due to the loading of six scissor lifts is shown in Fig. 6 for the beam and the drop. Also shown in Fig. 6 is the average crack spacing and maximum crack opening for each element. Comparing the cracking behavior of the beam and the drop it is evident that the cracking is much more

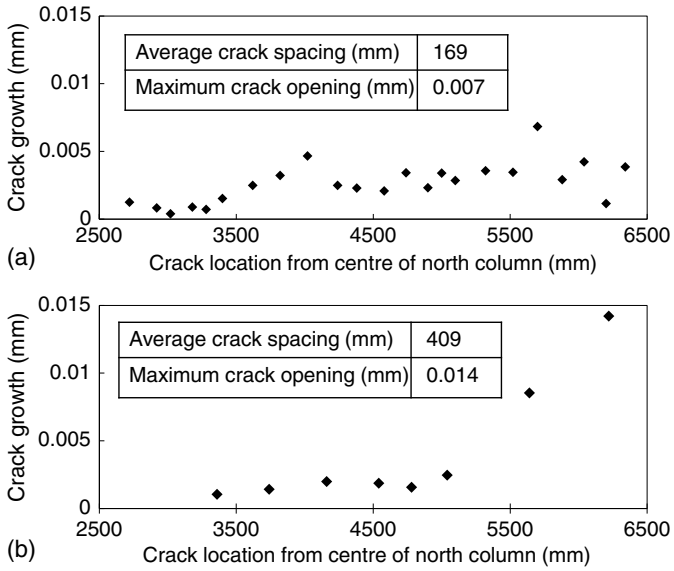

Fig. 6. Cracking behavior due to six scissor lifts at bottom fiber height: (a) beam; and (b) drop.

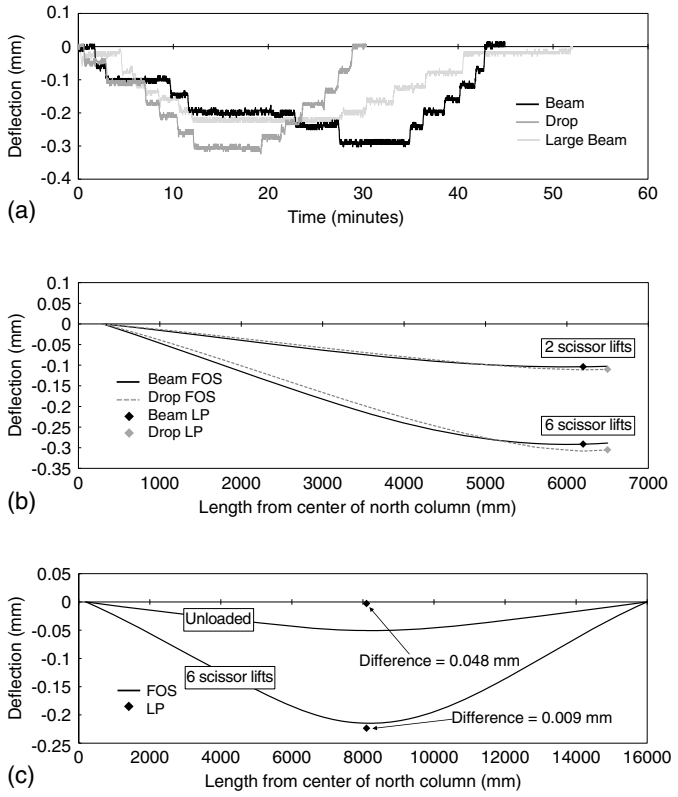

Fig. 7. Deflection behavior: (a) full load test LP measurements; (b) beam and drop deflected shape comparison; and (c) large beam deflected shape.

evenly distributed in the beam than in the drop. Using predictive equations from ACI 224R (ACI 2001) to determine the average crack spacing of an RC element in flexure, average crack spacings were predicted for the beam and drop to be 93 and 145 mm, respectively. Though the predicted values are lower than those measured in both cases, the fact that the average crack spacing in the drop is larger than in the beam is correctly predicted. This demonstrates the value in monitoring crack widths to ensure that serviceability criteria are not breached.

The FOS crack width measurement technique used cannot measure crack openings accurately that exceed 0.3 mm during testing (the allowable crack width for structures exposed to humidity, moist air, and soil is 0.30 mm in accordance with ACI 224R). If crack width increases larger than 0.3 mm are expected, the cracking behavior maps presented in Fig. 6 can still be of value in determining where cracks are located and which cracks are expected to have the largest widths. Using this information, discrete crack gauges can be placed in the appropriate locations (for instance, the two cracks near midspan of the drop) to accurately measure larger crack width increases.

Beam Deflections

Deflection versus time data is shown in Fig. 7(a) for the beam, the drop, and the large beam. The displacement measurements are from the linear potentiometers installed for each load test. For each element, the loading of all six scissor lifts one at a time is evident as steps in the deflection response. It is seen that the maximum deflection measured for the beam and the drop are very similar, with values of −0.291 and −0.305 mm, respectively. The maximum deflection reading during the large beam test is −0.223 mm. These deflection magnitudes are low, especially considering that even the most conservative deflection limitation in ACI 318 (ACI 2014a) of $l/480$ (where l is the span) equates to 27.1 mm for the beam and drop and 33.8 mm for the large beam. Note that the elements were not loaded to 100% of the unfactored design live load. However, if the approximation is made that the deflection response is linear after cracking up to the service load, deflection estimates for each element loaded to 100% of the unfactored design live load can be extrapolated. These deflection estimates are −0.77, −0.87, and −1.86 mm for the beam, the drop, and the large beam, respectively. These values are still much lower than the ACI 318-14 deflection limit for each element. Note that this particular deflection limit also considers time-dependent deflections (not measured in this study) from all sustained loads applied after nonstructural elements likely to be damaged by large deflections are installed in addition to immediate live load deflections.

The FOS installation layout on each element was configured so that strains would be measured at two separate heights on the element's length. Because the height difference between the top and bottom fibers was known in each case, curvature could be measured directly every 20 mm along each element's length anywhere that both the top and bottom fibers were installed. Using Bernoulli-Euler elastic beam theory, the measured curvatures can be integrated twice to determine bending deflections if two boundary conditions are known. The technique developed by Brault and Hoult (2018) to determine deflections from FOS strain measurements was used in this section, which was validated in the laboratory against conventional displacement sensors.

Fig. 7(b) shows the FOS distributed beam deflection measurements for the beam and the drop each loaded with two and six scissor lifts. For both the beam and the drop, the two boundary conditions used were the inner edge of the north column (bending deflection value of 0) and the displacement measurement taken from the LP. Because the FOS strain measurements were taken with a sensor spacing of 20 mm, each deflected shape shown in Fig. 7(b) is made up of 310 deflection points, illustrating that distributed deflections are captured with one fiber optic cable. The deflected shape provides insight into support conditions as well as where critical deflections occur. For instance, the maximum deflection

for both the beam and the drop does not occur at midspan (6,500 mm) but rather at 6,020 mm (−0.292 mm) for the beam and 6,200 mm (−0.308 mm) for the drop. Measuring the maximum deflection without knowing where it will occur prior to a test is a challenge with conventional discrete transducers, yet ACI 437R (ACI 2003) states that deflections should be measured at all critical points during a load test. Thus, the FOS technique is especially useful when in situ support conditions are unknown.

When comparing the deflected shapes of the beam and the drop, it can be seen that the response of both due to each loading scenario is very similar; however, the curvature of the drop appears to be more concentrated at midspan than is observed in the beam's deflected shape. This is consistent with the drop having two large cracks near midspan [Fig. 6(b)]. The maximum deflection of the beam is found to be 180 mm north of the drop's maximum deflection location. This is likely attributed to two things: (1) the drop's north support has a higher level of moment transfer than the beam's due to the drop extending 1.5 m beyond the north column, and (2) the resultant load of the six scissors lifts is 150 mm north of midspan for the beam and 90 mm south of midspan for the drop. Lastly, note that the beam and the drop were designed to have the same deflection response to vertical loading, which appears to be essentially the case.

The deflected shape of the large beam is shown in Fig. 7(c) when loaded with six scissor lifts as well as once the beam was unloaded. For the large beam, the two boundary conditions used were the inner edge of the north column (bending deflection value of 0 at 200 mm) and the inner edge of the south column (bending deflection value of 0 at 16,000 mm). As discussed, FOS strain measurements were not acquired at certain locations due to physical obstacles on the large beam, thus curvature could not be directly measured at every single point along the element's length. In order for the FOS deflection measurements to be performed in this case, linear interpolation of curvature was used where curvatures were not directly measured.

Because the LP displacement measurement was not used as a known boundary condition in the case of the large beam, the LP measurement could be used to compare and evaluate the bending deflections determined from the FOS data [as shown in Fig. 7(c)]. The magnitude of the LP displacement measurement is 0.009 mm larger than the FOS deflection measurement at 8,100 mm when the large beam is loaded with six scissor lifts. Note that the LP displacement measurement measures total displacement at this point, while the FOS deflection measurement only accounts for bending deflections. The larger LP displacement may be explained by axial deformations in the steel columns supporting the large beam when loaded. If the total scissor lift load (77.5 kN) is approximated to be evenly split between the north and south column (38.75 kN in each), then the axial deformation expected in each column can be determined using the cross-sectional area of each column (53,700 and 80,800 mm^2 for the north and south columns, respectively), the Young's modulus of the steel (200 GPa), and the column lengths (5,000 mm for both). The axial deformations expected in each column are 0.018 and 0.012 mm downward for the north and south columns, respectively. These values suggest that the discrepancies between the LP measurement and the FOS measurement at 8,100 mm may be caused by deformations of the columns. Note that the accuracy of the LP used is 0.024 mm, which is almost three times larger than the difference between the two measurement technologies. Overall the FOS measurements are in good agreement with the LP measurements.

It is evident in Fig. 7(c) that the LP measurement returns to 0 mm when the large beam is unloaded; however, the deflected shape measurement from the FOS at midspan does not (−0.048 mm). This suggests that the deflected shape measurement from the FOS is no longer correct once the beam is unloaded. To investigate why this is occurring, the FOS strain measurements from the top and bottom fibers of the large beam when unloaded were plotted as shown in Fig. 8.

Fig. 8 shows that the FOS strains return to approximately 0 $\mu\varepsilon$ between 0 and 4,000 mm, and again between 12,000 and 16,000 mm. However, between 4,000 and 12,000 mm there are still several strain peaks present ranging from 3 to 16 $\mu\varepsilon$. These strain peaks are located at crack locations where it appears irrecoverable strain is measured by the FOS despite the fact that the LP measurements show zero displacement (suggesting the cracks have returned to their initial width prior to testing). Thus, somewhere between the concrete surface and the fiber optic sensing core there appears to be irrecoverable deformations at cracks once the large beam is unloaded. A small-scale testing apparatus was fabricated (Fig. 9) to investigate whether the irrecoverable strains are specifically caused by the cracks, or whether they are caused by the magnitude of the measured strain and/or the large strain gradients measured surrounding the peaks.

The testing apparatus shown in Fig. 9 was comprised of two aluminum hollow structural sections (HSS) beams that were tightened together using threaded rods at either end of the beams with two steel rollers between them. By tightening the HSS beams together against the rollers, the rollers apply point loads to each HSS beam, which in turn subjects both HSS beams to 4-point bending. FOS were installed on one of the HSS beams 10 mm away from the extreme tension fiber using the same nylon coated fiber optic cable and epoxy used during the load tests. Two separate tests using the apparatus were performed. The first was performed with FOS installed on an intact HSS beam, and the second was performed with FOS installed on an HSS beam with a 25 mm long vertical cut at the beam's midspan to simulate a crack. In both instances, the beams were tightened against the rollers until the strain measured at the beam's midspan (where the cut was located) reached approximately 350 $\mu\varepsilon$ [Fig. 9(b)], which is larger than the maximum strain measured during the load tests of 200 $\mu\varepsilon$. The beams were then loosened away from the rollers (unloaded) and FOS

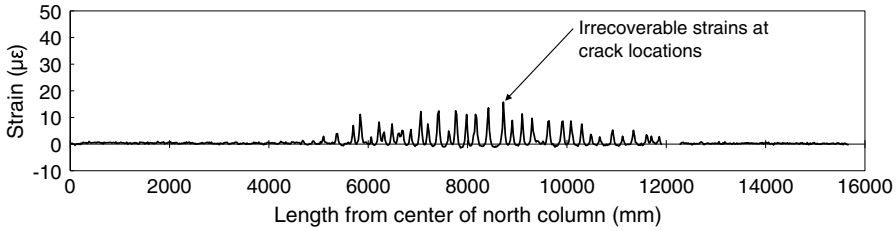

Fig. 8. Bottom fiber strain measurements for the large beam once unloaded.

J. Perform. Constr. Facil., 2019, 33(1): 04018096

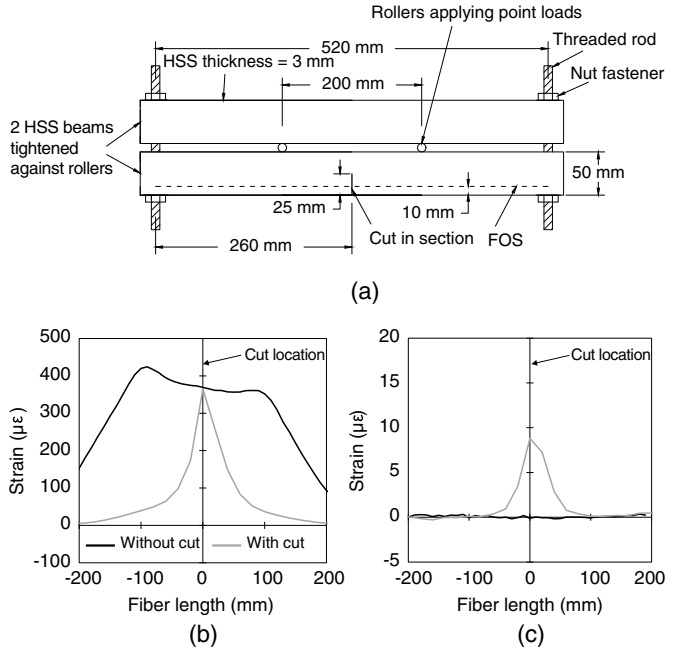

Fig. 9. Aluminum test apparatus: (a) apparatus schematic; (b) FOS strain measurements when loaded; and (c) FOS strain measurements when unloaded.

strains were measured to determine if any irrecoverable strains were present [Fig. 9(c)].

The strains induced in Fig. 9(b) are within the material's linear-elastic range, therefore the beam itself should not have any permanent deformations upon unloading. Thus, the irrecoverable strains would be within the fiber or the epoxy. This irrecoverable strain in the system is caused by one of the following: (1) a large strain magnitude, (2) a large strain gradient, or (3) a mechanism specific to crack opening. As shown in Fig. 9(b) the magnitude of the strains are equal at the cut location for both cases. The strain gradients induced are similar for both cases as well, though the shape of their strain profiles is different. Fig. 9(c) shows that the strains return to approximately 0 $\mu\varepsilon$ for the case without a cut, indicating that neither the strain magnitude nor the strain gradient measured when the beam was loaded lead to irrecoverable strains in the FOS system. However, the beam with a cut does still show a strain peak at the cut of 9 $\mu\varepsilon$ once unloaded (this peak value is within the range of irrecoverable strain peaks seen at crack locations in the load tests). This suggests that it is the concentrated opening of the cut (simulated crack) under loading which leads to irrecoverable strains in the FOS system upon unloading. Therefore, a current limitation of the FOS system used in this study is that it cannot accurately measure concrete behavior upon unloading if the FOS cross concrete cracks. Thus, further research is required to investigate this phenomenon before this particular FOS system is used to monitor cyclic or long-term behavior of concrete elements.

Design Model Comparison

The load configurations shown in Fig. 4 were applied to the structural models of each element that were used in the building's design. The beam and the large beam were modeled in S-line, which is a commercially available concrete beam design program created by S-frame. The drop was modeled in SAFE, which is a commercially available finite-element modeling software created by Computers and Structures, Inc. (CSI) for the design of concrete slabs. The maximum immediate live load deflections determined from the design models due to the scissor lift loading were −1.42, −1.51, and −0.84 mm for the beam, the drop, and the large beam, respectively. As discussed previously, the maximum deflections measured during each load test due to the scissor lift loading were −0.29, −0.31, and −0.21 mm for the beam, the drop, and the large beam, respectively. The maximum measured deflections are only 20%, 21%, and 25% of the values predicted for the beam, the drop, and the large beam, respectively. This suggests that there is beneficial structural behavior occurring in situ that is not predicted during design, which is a common finding when performing load tests on RC structures (Tumialan et al. 2014). What makes this case of particular interest is the robust data set that was captured during load testing from the distributed FOS. This level of detail can be used in a model updating exercise to help diagnose reasons for conservatism in design. The FOS used in this work were able to capture detailed cracking behavior (including crack opening), and deflected shapes in addition to distributed strains, which has never been done before in the field with this technology. Therefore, future work will aim to perform model updating using these uniquely detailed data sets to pin point the cause of discrepancies between current design predictions and measured behavior.

Conclusions

The current research program was performed to investigate the capabilities of distributed fiber optic sensors to monitor RC elements in situ during load testing. Two beams and one drop panel were load tested using the weight of six scissor lifts (average weight of 12.9 kN each). The elements were monitored with distributed FOS and linear potentiometers. The measurement accuracy of the FOS system used (~1 $\mu\varepsilon$) proved to be critical, as the strains induced during load testing remained between −6 and 202 $\mu\varepsilon$, with the majority of strains remaining between −6 and 50 $\mu\varepsilon$. The FOS strain measurements captured the positive bending and negative bending along the length of each element and allowed for the locations of each element's inflection points to be determined. This provided insight into support conditions, indicating the presence of moment transfer into either the columns or the surrounding floor slab at each support.

Along the entire length of the installed fiber optic cables, the location of the cracks as well as the amount that each crack had widened due to loading was determined. This information allowed the cracked regions of the RC element, the average crack spacing, and the maximum crack openings to be measured. The average crack spacings were compared to ACI 224R (ACI 2001) predictions. It was found that the predictions were on average 47% of the measured values. The maximum measured crack openings were 0.009 and 0.014 mm, occurring on the same element.

The deflected shape of each element when loaded was determined using the FOS measurements. It was found that the location and magnitude of the maximum deflection could be determined. This has advantages over discrete sensors when monitoring in situ, as the critical locations for measuring deflections are often not known prior to load testing. The maximum deflections measured for each element were compared to deflection predictions from each element's design model. It was found that the measured deflections were between 20% and 25% of the predicted deflection values, suggesting that there is beneficial structural behavior occurring in situ that is not accounted for in the models. Upon unloading, it was found that the FOS system no longer agreed with the LP measurements. An investigation determined that a certain level of irrecoverable strains occur in the FOS measurement system at crack

locations, causing the FOS measurements to lose accuracy when the element is unloaded. This is not a concern when loading the element; however, when unloading is also required to perform cyclic or long-term tests on RC structures further research is required.

Acknowledgments

The authors would like to thank the Natural Sciences and Engineering Research Council of Canada, the Ontario Ministry of Research and Innovation, the Canadian Foundation for Innovation, and Queen's University for financially supporting this study. The authors also thank Bryce Howchin, Blair Pearen, Tanner Blom, and Matthieu Marleau of PCL Construction, as well as Adam Hoag and Rebecca Garratt for their help with this research. Finally, the authors are indebted to Cadillac Fairview for granting permission for this research to be performed on site.

References

ACI (American Concrete Institute). 2001. *Control of cracking in concrete structures*. ACI 224R. Farmington Hills, MI: ACI.

ACI (American Concrete Institute). 2003. *Strength evaluation of existing concrete buildings*. ACI 437R. Farmington Hills, MI: ACI.

ACI (American Concrete Institute). 2008. *Guide for modeling and calculating shrinkage and creep in hardened concrete*. ACI 209.2R. Farmington Hills, MI: ACI.

ACI (American Concrete Institute). 2014a. *Building code requirements for structural concrete and commentary.* ACI 318. Farmington Hills, MI: ACI.

ACI (American Concrete Institute). 2014b. *Code requirements for load testing of existing structures and commentary.* ACI 437.2. Farmington Hills, MI: ACI.

Allwood, J., and J. Cullen. 2012. *Sustainable materials: With both eyes open*. Cambridge, UK: UIT Cambridge Limited.

Bastianini, F., F. Matta, A. Rizzo, N. Galati, and A. Nanni. 2007. "Overview of recent bridge monitoring applications using distributed Brillouin fiber optic sensors." *J. Nondestruct. Test.* 12 (9): 269–276.

Bentz, E. C., and N. A. Hoult. 2016. "Bridge model updating using distributed sensor data." *Proc. Inst. Civ. Eng. Bridge Eng.* 170 (1): 74–86. https://doi.org/10.1680/jbren.15.00030.

Billon, A., J. M. Hénault, M. Quiertant, F. Taillade, A. Khadour, R. P. Martin, and K. Benzarti. 2015. "Qualification of a distributed optical fiber sensor bonded to the surface of a concrete structure: A methodology to obtain quantitative strain measurements." *Smart Mater. Struct.* 24 (11): 115001 https://doi.org/10.1088/0964-1726/24/11/115001.

Bischoff, P. H. 2005. "Reevaluation of deflection prediction for concrete beams reinforced with steel and fiber reinforced polymer bars." *J. Struct. Eng.* 131 (5): 752–767. https://doi.org/10.1061/(ASCE)0733-9445(2005)131:5(752).

Brault, A., and N. A. Hoult. 2018. "Monitoring RC serviceability performance using fiber optic sensors." *ACI Struct. J.*, in press.

Casadei, P., R. Parretti, A. Nanni, and T. Heinze. 2005. "In situ load testing of parking garage reinforced concrete slabs: comparison between 24 h and cyclic load testing." *Pract. Period. Struct. Des. Constr.* 10 (1): 40–48. https://doi.org/10.1061/(ASCE)1084-0680(2005)10:1(40).

De Luca, A., H. J. Zadeh, and A. Nanni. 2013. "Assessment of performance of reinforced concrete strips by in-place load testing." *ACI Struct. J.* 110 (5): 813–821.

Galati, N., A. Nanni, G. Tumialan, and P. H. Ziehl. 2008. "In situ evaluation of two concrete slab systems. I: Load determination and loading procedure." *J. Perform. Constr. Facil.* 22 (4): 207–216. https://doi.org/10.1061/(ASCE)0887-3828(2008)22:4(207).

Gebremichael, Y., et al. 2005. "A field deployable, multiplexed Bragg grating sensor system used in an extensive highway bridge monitoring evaluation tests." *IEEE Sens. J.* 5 (3): 510–519. https://doi.org/10.1109/JSEN.2005.846185.

Gifford, D., S. Kreger, A. Sang, M. Froggatt, R. Duncan, M. Wolfe, and B. Soller. 2007. "Swept-wavelength interferometric interrogation of fiber Rayleigh scatter for distributed sensing applications." In *Fiber Optic Sensors and Applications V*, 67700F1. Bellingham, WA: SPIE.

Hoult, N. A., O. Ekim, and R. Regier. 2014. "Damage/deterioration detection for steel structures using distributed fiber optic strain sensors." *J. Eng. Mech.* 140 (12): 04014097. https://doi.org/10.1061/(ASCE)EM.1943-7889.0000812.

Li, H. N., D. S. Li, and G. B. Song. 2004. "Recent applications of fiber optic sensors to health monitoring in civil engineering." *Eng. Struct.* 26 (11): 1647–1657. https://doi.org/10.1016/j.engstruct.2004.05.018.

Lord Microstrain. 2015. "Subminiature gauging DVRT." Accessed May 6, 2015. http://www.microstrain.com/displacement/sg-dvrt.

Luna Technologies. 2011. *Optical backscatter reflectometer 4600 user guide*. Blacksburg, VA: Luna Technologies.

Maaskant, R., T. Alavie, R. M. Measures, G. Tadros, S. H. Rizkalla, and A. Guha-Thakurta. 1997. "Fiber-optic Bragg grating sensors for bridge monitoring." *Cem. Concr. Compos.* 19 (1): 21–33. https://doi.org/10.1016/S0958-9465(96)00040-6.

Majumder, M., T. K. Gangopadhyay, A. K. Chakraborty, K. Dasgupta, and D. K. Bhattacharya. 2008. "Fiber Bragg gratings in structural health monitoring: Present status and applications." *Sens. Actuators, A* 147 (1): 150–164. https://doi.org/10.1016/j.sna.2008.04.008.

Merzbacher, C. I., A. D. Kersey, and E. J. Friebele. 1996. "Fiber optic sensors in concrete structures: A review." *Smart Mater. Struct.* 5 (2): 196–208. https://doi.org/10.1088/0964-1726/5/2/008.

Minardo, A., G. Persichetti, G. Testa, L. Zeni, and R. Brenini. 2012. "Long term structural health monitoring by Brillouin fiber-optic sensing." *J. Geophys. Eng.* 9 (4): S64–S69. https://doi.org/10.1088/1742-2132/9/4/S64.

Mohamad, H., K. Soga, A. Pellew, and P. J. Bennett. 2011. "Performance monitoring of a secant-piled wall using distributed fiber optic strain sensing." *J. Geotech. Geoenviron. Eng.* 137 (12): 1236–1243. https://doi.org/10.1061/(ASCE)GT.1943-5606.0000543.

Ohno, H., H. Naruse, M. Kihara, and A. Shimada. 2001. "Industrial applications of the BOTDR optical fiber strain sensor." *Opt. Fiber Technol.* 7 (1): 45–64. https://doi.org/10.1006/ofte.2000.0344.

Regier, R. 2013. "Application of fiber optics on reinforced concrete structures to develop a structural health monitoring technique." M.A.Sc. dissertation, Dept. of Civil Engineering, Queen's Univ.

Regier, R., and N. Hoult. 2014. "Distributed strain behavior of a reinforced concrete bridge: Case study." *J. Bridge Eng.* 19 (12): 05014007. https://doi.org/10.1061/(ASCE)BE.1943-5592.0000637.

Regier, R., and N. Hoult. 2015. "Concrete deterioration detection using distributed sensors." *Proc. ICE Struct. Build.* 168 (2): 118–126. https://doi.org/10.1680/stbu.13.00070.

Scott, R. H., S. G. Gilbert, and R. M. Moss. 2002. "Load testing of floor slabs in a full scale reinforced concrete building." *Strain* 38 (2): 47–54. https://doi.org/10.1046/j.0039-2103.2002.00003.x.

Tumialan, G., N. Galati, and A. Nanni. 2014. "In-situ load testing of concrete structures. Part 1: Rationale, objectives, and execution." *Struct. Mag.* 10–12.

Vecchio, F. J., and M. P. Collins. 1986. "The modified compression-field theory for reinforced concrete elements subjected to shear." *ACI Struct. J.* 83 (2): 219–231.

Villalba, S., and J. R. Casas. 2013. "Application of optical fiber distributed sensing to health monitoring of concrete structures." *Mech. Syst. Sig. Process.* 39 (1–2): 441–451. https://doi.org/10.1016/j.ymssp.2012.01.027.